Journal of Volcanology and Geothermal Research 307 (2015) 68–78

Contents lists available at ScienceDirect

Journal of Volcanology and Geothermal Research

journal homepage: www.elsevier.com/locate/jvolgeores

Infrasound from the 2012–2013 Plosky Tolbachik, Kamchatka fissure eruption

Sarah Albert [a,*], David Fee [a], Pavel Firstov [b], Evgeniy Makhmudov [b], Pavel Izbekov [a]

[a] Wilson Infrasound Observatories, Alaska Volcano Observatory, Geophysical Institute, University of Alaska Fairbanks, Fairbanks, AK, USA
[b] Kamchatka Branch Geophysical Surveys, Petropavlovsk-Kamchatsky, Kamchatka, Russia

ARTICLE INFO

Article history:
Received 28 April 2015
Accepted 17 August 2015
Available online 31 August 2015

Keywords:
Infrasound
Monopole
Inversion
Emissions
Tolbachik
Volcano

ABSTRACT

We use both regional and local infrasound data to investigate the dynamics of the 2012–2013 eruption of Tolbachik Volcano, Kamchatka, Russia during select periods of time. Analysis of regional data recorded at the IMS array IS44 in southern Kamchatka, ~384 km from the vent focuses on the eruption onset in November 2012, while analysis of local data focuses on activity in February and August 2013. Signals recorded from Tolbachik suggest a change in eruptive intensity possibly occurred from November 27–30, 2012. Local infrasound data recorded at distances of 100–950 m from the vent are characterized primarily by repeated, transient explosion signals indicative of gas slug bursts. Three methods are employed to pick slug burst events in February and August. The nature of slug bursts makes a monopole acoustic source model particularly fitting, permitting volume outflux and slug radius calculations for individual events. Volume outfluxes and slug radii distributions provide three possible explanations for the eruption style of Tolbachik Volcano from mid-February to late August. Cumulative outflux for slug bursts (i.e. mass of emissions from individual bursts) derived by infrasound for both February and August range from <100 to ~3000 kg. These values are greater than infrasound-derived emissions calculated at Pacaya Volcano, but less than those calculated at Mt. Erebus Volcano. From this, we determine slug bursts at Tolbachik Volcano in February and August were larger on average than those at Pacaya Volcano in 2010, but smaller on average than those at Mt. Erebus in 2008. Our overall emissions estimates are in general agreement with estimates from satellite observations. This agreement supports the monopole source inversion as a potential method for estimating mass of emissions from slug burst events.

1. Introduction

Infrasound, or low frequency sound between ~0.02–20 Hz, has proven useful in the analysis and detection of volcanic eruptions. Volcano infrasound studies have given insight into eruption dynamics, including eruption type and estimates of emissions (Firstov, 1996; Johnson and Ripepe, 2011; Fee and Matoza, 2013). It is well known that atmospheric perturbations from various volcanic processes can produce characteristic infrasound signals. Exsolution of gases can produce both short duration explosions and longer duration tremor. More violent eruptions produce signals characteristic of volcanic jets and plumes (Fee and Matoza, 2013).

Local infrasound (collected <15 km from the source) and seismicity from short duration explosions have been studied extensively at various volcanoes including Sakurajima and Unzen Volcanoes in Japan (Yamasato, 1998; Garces et al., 1999), Soufriere Hills Volcano, Montserrat (Green and Neuberg, 2005), Mt. Etna, Italy (Gresta et al., 2004; Ulivieri et al., 2013), Arenal Volcano, Costa Rica (Hagerty et al., 2000), Mt. Erebus, Antarctica (Johnson et al., 2008), Shishaldin Volcano, Alaska (Vergniolle et al., 2004; Petersen and McNutt, 2007a), and Tungurahua Volcano, Ecuador (Ruiz et al., 2006; Kim et al., 2012). Some of these short duration explosions are the result of gas slug bursts. It was originally proposed that an explosion may occur when a bubble rises through the conduit and quickly undergoes expansion once it reaches a lower density zone (Buckingham and Garces, 1996). Additional infrasound-derived slug burst explosion models involve a rising gas slug oscillating at the surface of the lava lake and then bursting (Brandeis et al., 1994). While infrasound signals from slug bursts do vary, the typical impulse-like signal of an explosion consists of a compression (a wave which provides a large increase in pressure) followed by an almost equal rarefaction (an area of low pressure which follows). Similar slug burst events occurred during the recent 2012–2013 eruption of Tolbachik Volcano in Kamchatka, Russia.

Along with local infrasound from an eruption, regional infrasound data (collected ~15–500 km from the source) can be used to track changes in eruptive activity through time (Fee and Matoza, 2013). The Comprehensive Nuclear-Test-Ban Treaty (CTBT) was designed by the United Nations in 1996 to ban nuclear weapons testing and in turn created the International Monitoring System (IMS). The global IMS network consists of seismic, infrasound, hydroacoustic, and radionuclide

* Corresponding author at: Geophysical Institute, 903 Koyukuk Dr. Fairbanks, AK 99775, USA.
E-mail address: saalbert@alaska.edu (S. Albert).

http://dx.doi.org/10.1016/j.jvolgeores.2015.08.019
0377-0273/

sensors. Under preferential conditions, atmospheric waveguides and low attenuation allow infrasound to propagate far from the source, thus permitting global detection of volcanic eruptions using the IMS infrasound network. This network has proven particularly useful for the detection and characterization of remote eruptions (Fee and Matoza, 2013). One of the IMS infrasound arrays, IS44, is located in Kamchatka, Russia ~384 km south of Tolbachik Volcano (Fig. 1a). This array recorded infrasound signals near the onset time of the 2012–2013 eruption of Tolbachik Volcano.

In this manuscript we use local and regional infrasound data to gain insight into the eruption dynamics of Tolbachik Volcano. Data collected at the IMS array in Kamchatka, Russia provides constraints on the eruption onset. The presence or absence of an eruption signal at the regional infrasound array helps give insight into how energetic the eruption was in late November 2012. Local infrasound sensors, deployed hundreds of meters from the active vent in February and August 2013, recorded frequent, repetitive explosions. These repetitive explosions are assumed to be a result of near-continuous bursting of large gas slugs. The volume outflux from each gas slug burst can provide insight into the eruption size and how it changes through time. The nature of these gas slug bursts allows for the assumption of a "simple source", or a source "without any directional nature" (Lighthill, 1978). This type of source radiates pressure equally in all directions and is known as an acoustic monopole. Estimates of individual gas slug volume and size can be calculated when an acoustic monopole source model is assumed (Firstov and Kravchenko, 1996; Johnson et al., 2008; Dalton et al., 2010). By using the acoustic data acquired from this eruption we 1) explore the adequacy of slug burst event-picking methods, 2) estimate the total volume outflux of emissions and the slug radius for each event, and 3) identify any temporal changes in both the local and regional infrasound in order to better understand the dynamics of this particular eruption.

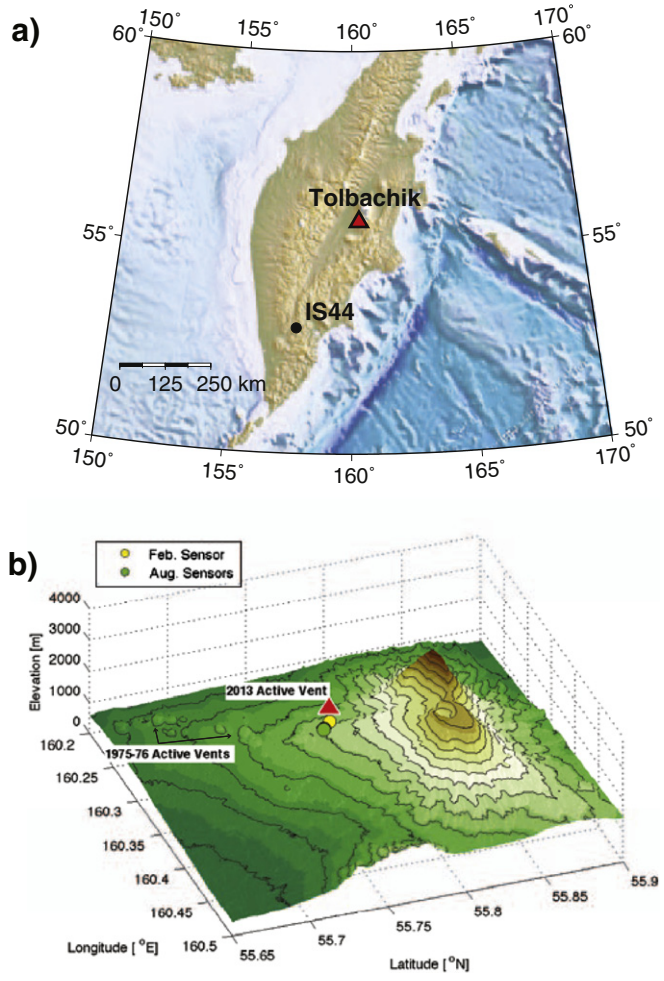

Fig. 1. Locations of a) Tolbachik Volcano and the International Monitoring Station IS44 infrasound array in Kamchatka, Russia and b) local sensors in February and August 2013 in reference to the active vent. Historical vents from the 1975–76 eruption are also labeled.

2. Tolbachik Volcano

The Tolbachik Volcanic complex, created 40,000–50,000 years ago, consists of two volcanoes: Ostry Tolbachik, a stratovolcano creating the highest peak, and Plosky Tolbachik, a shield volcano that lies east of the summit (Fedotov et al., 2011). Currently, only Plosky Tolbachik is active and is referred to as "Tolbachik Volcano" or "Tolbachik" in this paper, as it is commonly referred. Tolbachik Volcano lies 3085 m above sea level and is characterized by a summit caldera ~3.5 km in diameter. There are two zones of cinder cones, which formed ~10,000 years ago. These zones reach out 20 km to the northeast and 50 km to the southwest of the volcano's summit. The magmatic plumbing system stems from the Klyuchevskoy Volcano Group and is characterized by a magma chamber that lies directly below Tolbachik Volcano at a depth of ~2 km and with a volume of 40–70 km^3 (Fedotov et al., 2011).

The most recent activity at Tolbachik Volcano is characterized by large eruptions in 1941, 1975–76, and 2012–13. The 1975–76 eruption was very large, being referred to as "The Great Tolbachik Fissure Eruption". It began in late June 1975 as weak explosions from the summit crater. Just over a week later, three cones began to form southwest of the summit along with fissure activity (Fig. 1b). Activity lasted ~72 days, producing a total erupted volume of 1.18 km^3, consisting of tephra deposits and lavas. This eruptive activity was similar to the activity that occurred in 1941 (Braitseva et al., 1997; Fedotov et al., 2011; Inbar et al., 2011). During the 1975–76 eruption, another cone also formed south of the first three (Fig. 1b). Weak Strombolian-type activity at the southern cone, superimposed on the continuous effusive activity, lasted for ~450 days. This single cone produced 0.968 km^3 of lava (Fedotov et al., 2011; Inbar et al., 2011). The 2012–2013 eruption of Tolbachik Volcano was no exception to the historical activity. It began as a fissure eruption at 5:15 UTC on November 27, 2012 and continued into late September 2013, though most of the activity occurred before August 24, 2013 (Gordeev et al., 2013a; Zelenski et al., 2014). After a few days the fissure eruption transitioned to a discrete vent along the volcano's flanks. By December the eruption had largely transitioned to a second discrete vent where Strombolian activity dominated. Each vent produced a lava flow. By December 13, 2012, Gordeev et al. (2013b) estimate volumes of erupted lavas from both vents to be 0.0207 km^3 and 0.208 km^3, respectively. During the eruption a lava lake was also present in the crater. Slug bursts were frequent within the lava lake (Gordeev et al., 2013a; Zelenski et al., 2014). Preliminary calculations by Gordeev et al. (2013b) that estimate the average mass outflux of emissions from slug bursts in February 2012 were ~250 kg/s. During this time, visual observations suggest that explosions occurred every 3–5 s on average.

3. Data

3.1. Local infrasound

In collaboration with the Kamchatka Branch Geophysical Surveys (KBGS) and Institute of Volcanology and Seismology (IVS), a single National Center for Physical Acoustics (NCPA) infrasound sensor placed ~100 m from the active vent collected data from February 12–14, 2013 (Fig. 1b). This sensor uses piezo-ceramic sensing elements with a 24-bit digitizer. Timing is given by Global Positioning System. The sensors have a flat frequency response between ~0.02–250 Hz and can reach pressures of ±1190 Pa. Three Hakusan Corporation infrasound sensors (models SI102 and SI103) located ~825–955 m from the vent collected

data from August 14–20, 2013, though not continuously (Fig. 1b). Recording length is a result of both sensor battery capacity and technician/terrain accessibility. Both Hakusan Co. models have a flat frequency response between ~0.1–1000 Hz. During both deployments a lava lake was present in the active crater. Slug bursts occurred in the lava lake and are confirmed by video data collected in Feb. 12–14, by visual observations (Fig. 2), and are seen in the infrasound data by their characteristic shape (Fig. 3). Local infrasound data shows repetitive bursts occurring frequently with varying amplitudes (Fig. 3). Similarities are present between this data and acoustic signals from Mt. Etna in 2006–2013 (Ulivieri et al., 2013). During this period, Mt. Etna produced repetitive explosions similar to those occurring at Tolbachik Volcano in mid-February and late August 2013, but with much higher amplitudes. These repetitive explosions are assumed to be the result of near-continuous gas slug bursts.

Our data and analyses are primarily limited by single sensor data in February. Therefore, it was necessary to explore various filtering and cross correlation methods to extract information on the eruption dynamics. We experimented with band-pass and high-pass filtering methods and examined cross correlation values between sensors in three August datasets. A windowed cross correlation method was implemented to find events in both the August and February data using a master waveform. These methods are further detailed in Section 4.1.

3.2. Regional infrasound

Regional data were recorded by the IMS array, IS44, located in southern Kamchatka, Russia (Fig. 1a). IS44 is located ~384 km to the southwest of Tolbachik Volcano. The array recorded continuous data before the eruption, during the eruption from November 27, 2012 through September 2013, and after September 2013. This manuscript, however, focuses on only the data collected at the IS44 array during the first few days of the Tolbachik eruption, November 27–30, 2012. The IMS data are contaminated by wind so the pure-state filter is employed to remove noise (Olson, 2004). The usage of the pure-state filter is further detailed in Section 4.2.

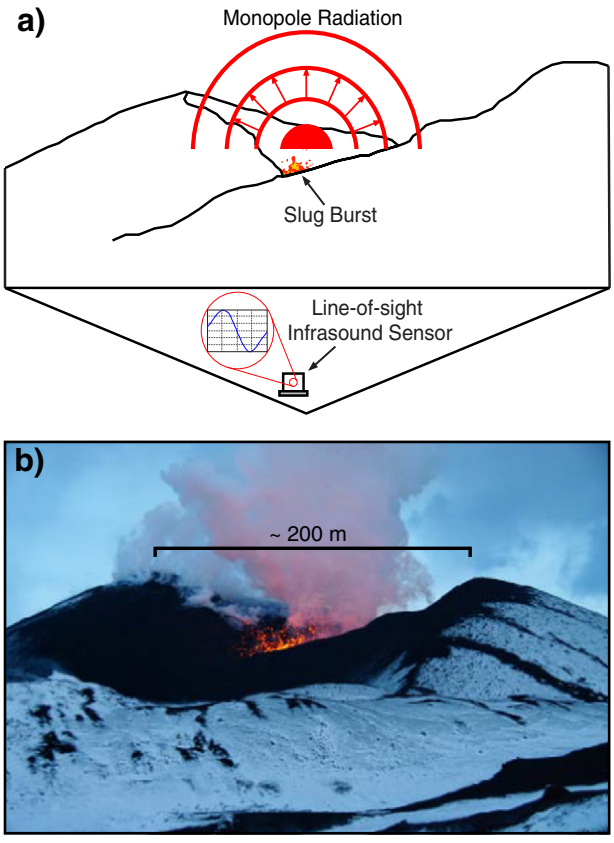

Fig. 2. Tolbachik's active vent. a) Monopole point source model and radiation pattern. The slug burst acts as a point source from which acoustic waves radiate equally in all directions. The line-of-sight infrasound sensor allows for direct collection of waveforms from the source. Slug burst explosions create simple, sinusoidal, waveforms as shown in the circle emanating from the sensor. b) A picture of a slug burst occurring at the active vent in February 2013.

4. Methods

4.1. Local infrasound analysis

4.1.1. Explosion picking methods

Three-sensor data from August allows us to explore filtering and cross correlation methods to detect slug burst events and to determine the accuracy of event picking in February. The repetitive nature and similarity of the explosions allowed for the use of a windowed cross correlation (WXC) method on both the February and August datasets. This method isolates explosive events in each dataset from a ~1 second "master" waveform (Anstey, 1964; Petersen, 2007; Petersen and McNutt, 2007a; Petersen and McNutt, 2007b). The master waveform is chosen to be characteristic of the explosion data in that it exhibits the typical compression and rarefaction signals of a slug burst (Figs. 2a, 3). Concurrent video was taken during the collection of the February data and was used to identify a master waveform for that time period. August data did not have accompanying video, therefore a waveform with a high correlation value between all three time-aligned sensors was chosen as the master. After identification, the master waveform is cross-correlated across the data in 1 second windows with 50% overlap. The short time window is necessary to capture individual events. Windows that produced a cross correlation value of 0.9 or greater are chosen as slug burst events from Tolbachik Volcano.

Due to the availability of three-sensor data in August 2013, two other filtering methods were employed on this data set for event picking. This was done to test the accuracy of the WXC method, as that is the only event picking method used in February due to limitations of single-sensor data. Because three sensors collected data in August, we could time-align and cross correlate the signals in ~1 s windows across sensors to determine explosive events. Prior to time-aligning and cross correlating the signals from all sensors, we experimented with two types of filtering. For the first filtering method, we chose to band-pass filter the data between 0.5–5 Hz in order to avoid signal contamination from the microbarom (~0.2 Hz signals that occur from natural processes related to ocean waves) (Donn and Rind, 1972). The second type of filter, a high-pass filter (>5 Hz), was experimented with due to the increased signal-to-noise ratio of slug bursts at higher frequencies. After filtering the data, windowed cross correlation was performed across all three sensors using a ~1 second window with 50% overlap. Again, it is important to note here that a master waveform is not used in this process, but rather the signal is cross correlated for each sensor pair. The mean from all three sensor cross correlation pairs is taken for each window. Windows that produced a mean cross correlation value of 0.9 or greater are chosen as slug burst events. For the duration of this paper these filtering and explosion picking methods will be referred to as the BPSC (Band-pass Filter and Sensor Cross Correlation) and HPSC (High-pass Filter and Sensor Cross Correlation) methods. It is important to note that the BPSC and HPSC methods are unique to the August data because of the availability of three-sensor data. A summary of the explosion picking methods can be found in Table 1.

4.1.2. Monopole source modeling

During February and August 2013, explosions from Tolbachik Volcano's discrete vent generally produced simple, impulsive, signals (Fig. 3). These signals were a product of atmospheric acceleration and

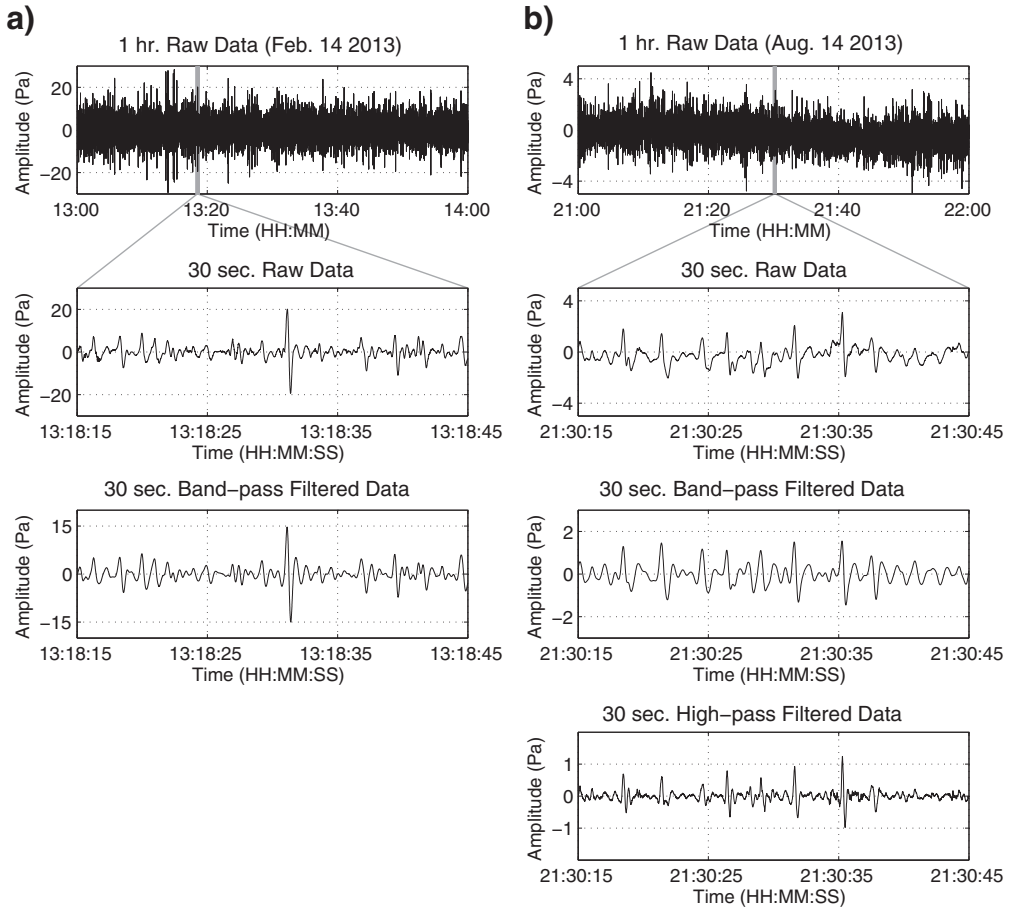

Fig. 3. Sample of raw and filtered infrasound data recorded a) February 14, 2013 and b) August 14, 2013. Data are characterized by frequent slug burst events that produce repeated short-duration infrasound signals. 1 hour segments of raw data for both February and August are characterized by many short duration events. 30 second raw and filtered samples of data show events that display the characteristic shape of slug bursts with varying amplitudes. Band-pass filtering data for February makes slug burst events more evident. Both band-pass and high-pass filtering data in August makes slug burst events more evident.

can be likened to the bursting of a spherical balloon or a "symmetric chemical explosion" (Johnson et al., 2008). Fig. 2 shows a schematic of the slug burst process and the expected acoustic waveform. The simplicity of the waveforms and the assumed source process (repeated slug bursts) makes a monopole source model particularly fitting for our analysis (Firstov and Kravchenko, 1996; Johnson et al., 2003; Johnson et al., 2008; Dalton et al., 2010). In some volcanic contexts the acoustic radiation from an eruption is not completely defined by a monopole source, but rather a combination of monopole and dipole sources. Kim et al. (2012) made use of this "multipole" source model at Tungurahua Volcano, Ecuador and found reliable estimates of volume outfluxes from explosive events with high signal-to-noise ratios. Explosions at Tungurahua Volcano are larger and more complex than the activity described in our study. Therefore, we assume that the eruptive source contains only a monopole component due to the simple nature of the slug burst events at Tolbachik Volcano. The far-field excess pressure radiated by a monopole source is given by the equation:

$$p - p_0 = \frac{\dot{q}\left(t - {}^{r}/_{c}\right)}{4\pi r} \tag{1}$$

where $p - p_0$ represents the excess pressure recorded by the acoustic sensor, $\dot{q}\left(t - {}^{r}/_{c}\right)$ represents the first derivative of the mass outflux (also known as the monopole source strength) at time $t - {}^{r}/_{c}$, r is the distance from the source to the sensor, and c is the speed of sound (~0.344 km/s) (Lighthill, 1978). For our experiment the speed of sound is determined from delay-and-sum beamforming for the highest signal power in August 2013. The volcanic context does not allow for complete spherical pressure radiation because of the Earth's surface. Therefore, a half space model is employed (using only half of the sphere) and the denominator of the monopole equation becomes $2\pi r$. From Eq. (1), it is easy to see that the source strength, $\dot{q}$, can be solved for directly from the acoustic data. $\dot{q}$ (kg/s^2) is then integrated once to find the mass outflux (kg/s) and then again to find the cumulative mass outflux (kg).

It is perhaps easier to visualize the amount of emissions from each explosion as volume outflux rather than as cumulative mass outflux. Total volume outflux of emissions can be related to the cumulative mass outflux by the following equation:

$$Q = \frac{1}{\rho_{air}} S(t) \tag{2}$$

where Q is total volume outflux, $\rho_{air} = 1.14$ kg/m^3 (at 1500 m above sea level and 20 °C), and S(t) is cumulative mass outflux for a particular explosion (Kim et al., 2012). Cumulative mass outfluxes were converted to total emission volumes for each explosion and the equation for the volume of a sphere was employed to solve for the individual slug radius, assuming the slug exploded as a spherical bubble (Johnson et al., 2008; Dalton et al., 2010).

4.2. Regional infrasound analysis

We analyze regional infrasound data from November 27–30, 2012. The data were first band-pass filtered between 0.5–5 Hz in order to remove microbarom effects. Upon band-pass filtering the data, the pure-

Table 1
Summary of explosion picking methods used on the February and August data sets.

Method	Acronym	Data set(s) implemented on	Filtering limits	Cross correlation across sensors	Usage of master waveform	Cross correlation threshold
Windowed cross correlation	WXC	February August (all)	0.5–5 Hz	No	Yes	0.9
Band-pass filter and sensor cross correlation	BPSC	August (all)	0.5–5 Hz	Yes	No	0.9
High-pass filter and sensor cross correlation	HPSC	August (all)	>5 Hz	Yes	No	0.9

state filter was employed to reduce background noise. This filtering method was chosen because of its effectiveness in filtering isotropic, uncorrelated, noise usually seen in infrasound array data. The spectral matrix from the data (the outer product of the Fourier transform of the time series data and its Hermitian conjugate) is used to estimate the degree of polarization, or "generalized coherence". Data with a high degree of polarization, P^2, are treated as coherent and are unperturbed by the filter. In turn, frequencies with a low P^2 value, or those characterized by noise, are suppressed (Olson, 2004).

After filtering, signal back-azimuths and trace velocities as well as a measure of signal-to-noise ratio (Fisher Statistic) were calculated in order to find infrasound signals from Tolbachik Volcano. Least squares estimation was implemented to find the back-azimuths and trace velocities of plane wave acoustic signals traversing the array in 20 s windows with 50% overlap (Szuberla and Olson, 2004). The Fisher Statistic (F-statistic) was used to give a measure of the signal-to-noise ratio and was also computed for each 20 second window. The F-statistic is related to the signal-to-noise ratio (SNR) by $SNR = (F\text{-}statistic - 1)/N$, where N is the number of samples (Blandford, 1974). A SNR threshold of 1 (i.e. F > 5), back-azimuth of 27 ± 8°, and trace velocity of 0.34 ± 0.10 km/s were used in order to identify time windows with signals originating from Tolbachik Volcano.

5. Results

5.1. Comparison of explosion-picking methods

The WXC, BPSC, and HPSC methods were experimented with in order to identify slug burst events within the three August datasets, and to examine the adequacy of the WXC method used in the February dataset. Fig. 4 shows a comparison of probability density functions (PDFs) of the selected waveforms for the February data and each of the August datasets using each filtering method. The beginning date of each dataset and the explosion picking methods are denoted in the title of each plot. The numbers in each plot correspond to the cross correlation value between the highest probability line (white dashed line) and the master waveform (black dashed line) used in the WXC method for that data. 95% confidence intervals for the waveform probability densities are shown as gray lines. The master waveforms from the WXC method are plotted as a reference of how well the highest probability matches an actual event. Amplitudes are normalized.

5.2. Total emissions values

We now investigate the timing between slug burst events. Video observations made ~100 m from the vent in February give estimates that slug burst explosions occurred every 3–5 s. The WXC method suggests an average number of ~1910 explosions per hour, which translates into a recurrence interval of 1.9 s per explosion (Fig. 5). The three methods employed in the August data show average number of explosions per hour ranging from 345–5560, or recurrence intervals ranging from every 0.6 s up to every 10 s depending on the method (Fig. 5). The number of events per hour stays relatively consistent for all four datasets when the WXC method is employed (Fig. 5a). Both the BPSC and HPSC methods show noticeable variations (Fig. 5b–c). The WXC method shows the most consistency with on average 1910, 2610, 2470, and 2210 explosions per hour (every 1.9 s, 1.4 s, 1.5 s, and 1.6 s) for the data beginning February 12, August 14, August 16, and August 19 respectively. The highest variance for the average number of explosions occurring per hour results from the HPSC method. This method gives average values of 3190, 1400, 345 explosions per hour (every 1.1 s, 2.6 s, and 10 s) for the data beginning on August 14, August 16, and August 19. The BPSC method gives average values of 5560, 3160, and 1330 explosions per hour, or every 0.6 s, 1.1 s, and 2.7 s for the data beginning August 14, August 16, and August 19 respectively. A comprehensive list of total number of explosions, average number of explosions per hour, and average recurrence intervals per hour is displayed in Table 2.

We now estimate the total volume outflux of emissions and solve for gas slug radius for each event found in the four datasets using the WXC, BPSC, and HPSC methods. Fig. 6a shows the total volume outflux per hour from the events identified using the WXC method, while Fig. 6b–c shows the same calculations using the BPSC and HPSC methods. Similar trends are present in the total volume outflux as in the number of explosions (Figs. 5 and 6). When the WXC method is employed, the total volume outflux per event stays relatively stable for each dataset. The BPSC and HPSC methods show that the highest total volume outflux per hour generally results from the data beginning August 14, 2013 while the lowest total volume outflux per hour results from the data beginning August 19, 2013 (Fig. 6b–c). A comprehensive list of cumulative mass outflux and total volume outflux is displayed in Table 2. Cumulative mass outflux is included as it was used to calculate total volume outflux of emissions using Eq. (2).

Slug radii values were calculated for each event. Fig. 7a–c shows the distribution of slug radii values for the three methods. In these plots the August data are represented by blue bars and have been grouped into one distribution because of their proximity in time. Even though the WXC method was the only method employed on the February data, the distribution of radii values are plotted as red bars in each plot for use as a reference. Radii values calculated from events picked using the WXC method show a normal distribution with a mean of 3.36 m and 3.76 m for the February and August data respectively. The BPSC and HPSC methods produced many radii values that fall near zero. The smallest mean radii value for the August data comes out of the usage of the BPSC method and is 2.77 m. The HPSC method falls in the middle, giving a mean slug radii size of 3.51 m. Table 2 provides a comprehensive list of the total number of explosions, average number of explosions per hour, cumulative mass outfluxes, total volume outfluxes, and mean slug radii values for the February and August datasets and methods.

5.3. Results from regional infrasound

Array processing results from least squares and F-statistic analysis show numerous infrasound signals from Tolbachik Volcano detected at IS44 between November 28–29, 2012 (Fig. 8). It is known from seismic observations that the eruption began at approximately 05:15 UTC on November 27, 2012 and that the fissure eruption transitioned to a discrete vent within a few days (Gordeev et al., 2013a; Zelenski et al., 2014). A trace velocity of 0.34 ± 0.1 km/s and a back azimuth of 27 ± 8° are expected for signals from Tolbachik Volcano. No clear infrasound arrivals are detected at IS44 on November 27 (Fig. 8). Therefore, the eruption onset cannot be seen in the regional infrasound data.

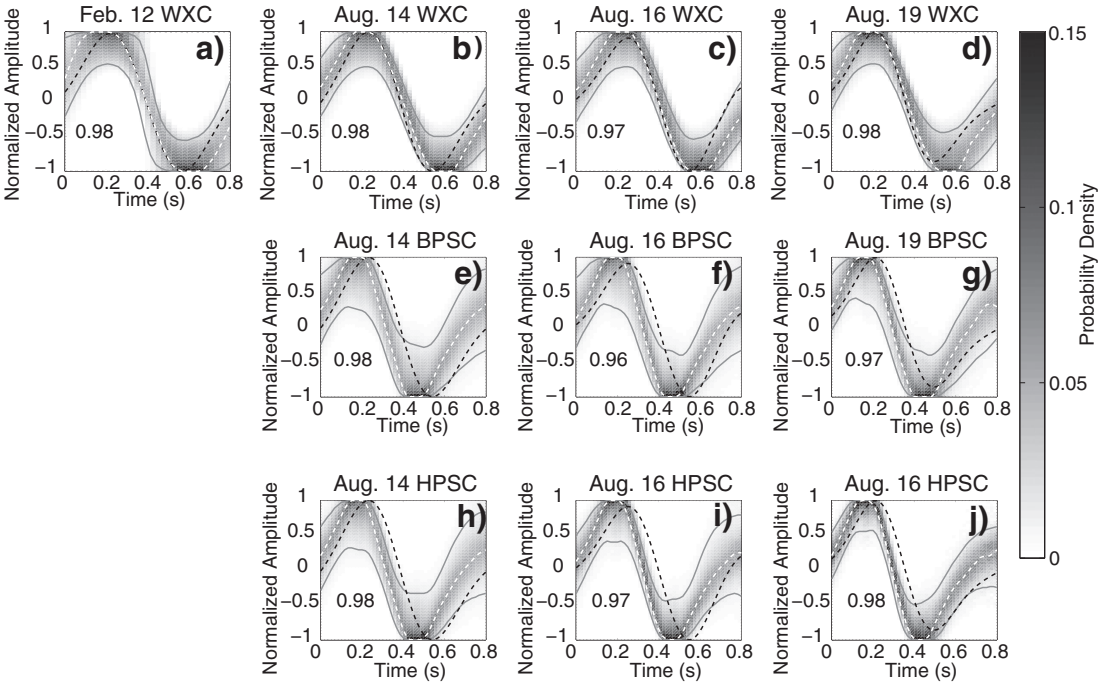

Fig. 4. Comparison of probability density functions (PDF) of the selected waveforms for each data set and explosion-picking method. The beginning date of each dataset and the explosion picking methods are denoted in the title of each plot. The numbers in each plot correspond to the cross correlation value between the highest probability line (white dashed line) and the master waveform (black dashed line) used in the WXC method for that data. 95% confidence intervals for the waveform probability densities are shown as gray lines. Amplitudes are normalized. The highest probabilities derived from each PDF both qualitatively and quantitatively match their corresponding WXC master waveforms well.

However, signals with the correct trace velocities and back-azimuths for Tolbachik Volcano, as well as relatively high SNRs, are evident November 28 beginning around 0000 UTC and continue into early November 29, 2012 (Fig. 8b–c). Filtered infrasound amplitudes during these periods are generally quite low (<0.1 Pa).

6. Discussion

6.1. Adequacy of explosion picking methods

PDFs of events picked using the WXC method (Fig. 4a–d) generally show waveforms characteristic of slug bursts as suggested by their simple and sinusoidal shape. A compression and a relatively equal rarefaction can be seen in all highest probability lines. The highest probabilities derived from each PDF both qualitatively and quantitatively match their corresponding WXC master waveforms well. This can be seen in the very high cross correlation values present between the highest probability lines and the WXC master waveforms from each dataset (all above 0.95) (Fig. 4a–j). Also, the WXC master waveforms either entirely or almost entirely lie within the 95% confidence limits of the probability densities for each dataset and method. Qualitatively, it is easy to see a compression and a relatively equal rarefaction in the highest probability lines (Fig. 4a–j). From these results we determine that all explosion picking methods identify actual slug burst events from the Tolbachik eruption, with the BPSC and HPSC methods identifying many smaller slug bursts. Therefore, regardless of the method, number of explosions and cumulative outflux of emissions are representative of the Tolbachik eruption for the February and August time periods. Explosion picking methods that identify a smaller number of events overall (the WXC and HPSC methods) can serve as a lower bound for number of explosions and cumulative outflux of emissions.

Possible sources of error in the explosion picking methods include the short window length and picking of non-slug burst events or other non-volcanic infrasound signals, though we believe the latter is unlikely. A longer window length is usually preferable because it allows for the cross correlation of more information. However, the 1 second window length was necessary for identifying slug burst events due to the simplicity of the signal. In our study, non-slug burst events may be attributed to roiling within the lava lake, especially when using the BPSC and HPSC methods. Roiling of a lava lake degassing has been found to be a significant source of infrasound (Fee and Matoza, 2013). However, roiling of the lava lake is likely a combination of many small slug burst events. Therefore, the total volume of emissions from roiling within the lava lake can be estimated using the monopole source inversion method described above.

Even though sources of error are possibly present, the high cross correlation values between the highest probability lines and the actual events suggest most events were identified correctly. Both the BPSC and HPSC methods identify smaller events, as seen in the distribution of slug radii sizes. Due to the high cross correlation value between the sensors, we deduce that these small events may be related to roiling within the lava lake as a result of persistent degassing. Because of the likelihood that all events detected in the three methods are indeed actual volcanic degassing events, the next section explores three possible eruption styles from mid-February to late August 2013: 1) the eruption stays consistent through time, 2) the eruption transitions from dominantly slug bursts in February to a mixture of roiling within the lava lake and slug bursting in August, or 3) the eruption transitions from dominantly slug bursts in February to a mixture of roiling within the lava lake and slug bursting in August, but fewer explosions occur overall.

6.2. Eruption characteristics through time

Regional infrasound analyses can give insight into eruption dynamics at the beginning of the eruption. Results from this study are particularly promising for regional infrasound interpretation between November 28 and early November 29, 2012. It is known from visual observations that lava flows occurred from two centers and ash emissions were occurring at Tolbachik Volcano during this period (Gordeev et al., 2013a). The relatively high SNR at this time along with the back-azimuths and trace velocities suggest signals from Tolbachik Volcano were picked up

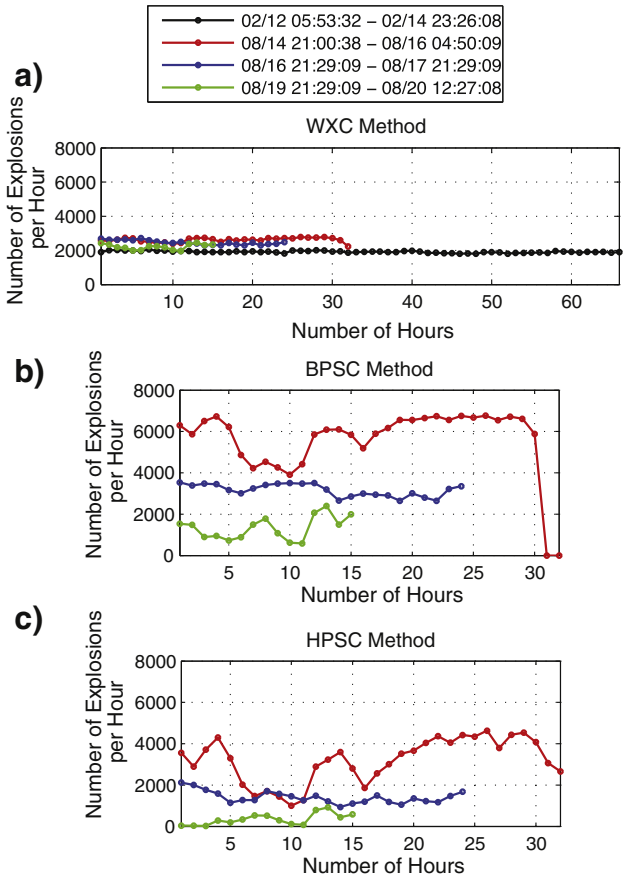

Fig. 5. Number of explosions per hour for datasets using the following methods: a) WXC, b) BPSC, and c) HPSC. The WXC method shows a relatively consistent trend for all datasets. The BPSC and HPSC methods show noticeable decreases in number of explosions per hour for the August 16–20 datasets. Table 1 provides a comprehensive list of the average number of explosions per hour and the recurrence intervals for each data set and method.

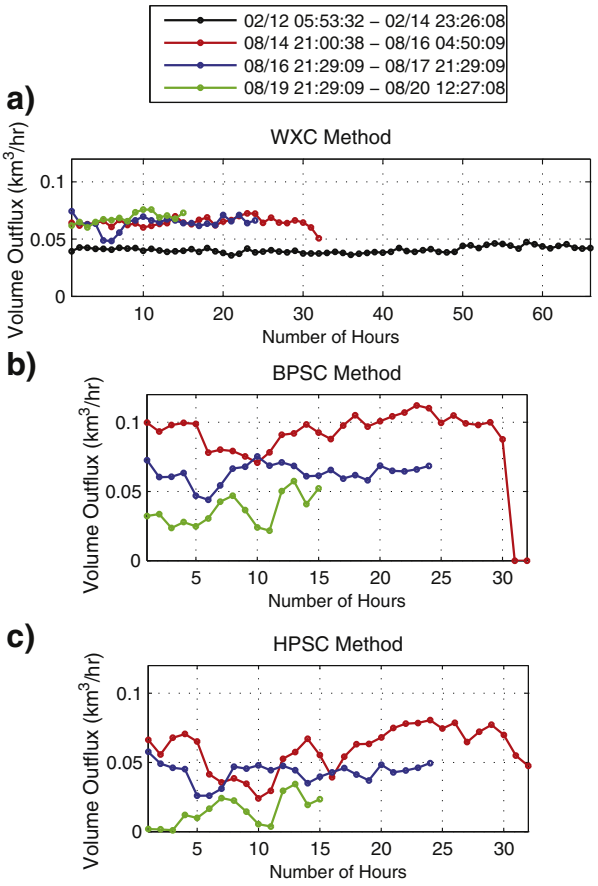

Fig. 6. Total volume outflux of emissions per hour using the following methods: a) WXC, b) BPSC, and c) HPSC. As in Fig. 5, the WXC method shows a relatively consistent trend for all datasets, whereas the BPSC and HPSC methods show noticeable decreases in total volume outflux per hour for the August 16–20 datasets. Table 1 provides a comprehensive list of the total volume outflux per hour for each dataset and method.

at the IS44 array between November 28 00:00–November 29 2:00 UTC. November 29–30 shows fewer events from Tolbachik Volcano.

The eruption onset time, derived from seismic observations, is not seen in our regional infrasound data. This suggests that it was not energetic enough for acoustic signals to propagate large distances (Fee and Matoza, 2013). Signals from Tolbachik Volcano are observed on November 28 to early November 29. Signal amplitudes are low so we use back-azimuth, trace velocity, and F-statistic calculations to determine signal presence. Noise levels during November 27–30 are similar for all days. Because signals from Tolbachik Volcano are seen in the regional data on November 28 to early November 29 and noise levels are consistent, the eruption likely increased in intensity during this period. The eruptive intensity must have returned to lower levels on November 30 because the signal is no longer seen. It is unlikely that atmospheric conditions changed drastically enough to result in the detection of the signal at the IMS station on November 28–29. However, future detailed acoustic propagation modeling could give more detailed information into signal propagation from the volcano to the infrasound array on November 27 and 30. However, current results provide evidence for an increase in eruptive intensity from November 28 to early November 29, 2012.

Of the three methods employed on the local infrasound data, the WXC method shows the least change through time. Data from the WXC method suggests the number of explosions per hour, the total

Table 2
Explosion data and monopole calculations from the three explosion picking methods and various datasets. While not continuous, the August data have been grouped because of their nearness in time.

Data	Method	Number of explosions	Average number of explosions per hour	Average recurrence interval (s)	Cumulative mass outflux, entire time period (kt)	Total volume outflux, entire time period (km^3)	Average slug radius (m)
02/12 05:53:32–02/14 23:26:08	WXC	241,765	1913	1.9	38	0.033	3.36
08/14 21:00:38–08/16 04:50:09	WXC	83,776	2618	1.4	24	0.021	3.65
	BPSC	177,969	5562	0.6	32	0.028	2.45
	HPSC	102,209	3194	1.6	22	0.019	2.73
08/16 21:29:09–08/17 21:29:09	WXC	59,150	2465	1.5	17	0.015	3.71
	BPSC	75,824	3159	1.1	17	0.015	2.77
	HPSC	33,730	1405	2.7	11	0.010	3.63
08/19 21:29:09–08/20 12:27:08	WXC	33,217	2215	1.6	11	0.010	3.92
	BPSC	19,962	1331	2.6	6	0.0055	3.09
	HPSC	5173	345	10.	3	0.0022	4.16

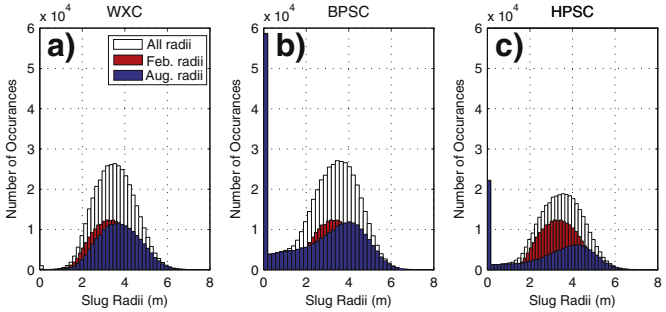

Fig. 7. Slug radii distribution for the a) WXC, b) BPSC, and c) HPSC methods. The distribution of the total calculated radii for each method is displayed by the white bars. The distribution of the February radii values calculated from the WXC method are displayed by the red bars, while the August radii values calculated using the BPSC and HPSC methods are displayed in blue. August radii calculations have been grouped due to the proximity in time of the datasets. Radii values calculated from events picked using the WXC method show a normal distribution with a mean of 3.36 m and 3.76 m for the February and August datasets, respectively. The BPSC and HPSC methods produced many radii values that fall near zero. The smallest mean radii value for the August dataset originates from the BPSC method and is 2.77 m. The HPSC method falls in the middle, giving a mean slug radii of 3.51 m.

volume of emissions, and the slug radii size stayed consistent from February to August (Figs. 5a, 6a, and 7a). Thus, these results suggest there was no change in the eruption from mid February 2013 to late August 2013. However, video and other observations from February and August suggest the eruption did change significantly. Video data from February could only be taken at a distance because of the large and frequent explosions. Even so, discrete, large, explosions can clearly be observed. Video from August could be taken from the edge of the vent and shows smaller slug bursts and roiling within the lava lake. The consistency in the number of explosions and total volume of emissions through time occurs because this method ignores other signals produced from the lava lake. Unlike the other BPSC and HPSC methods, the WXC method only searches for signals that resemble large slug burst events. Because this method shows consistency in radii sizes through time and only identifies large slug bursts, the WXC method likely underestimates the total volume outflux in all data, but serves as a lower bound.

Alternatively, the BPSC method shows numerous small amplitude events along with a larger number of slug burst explosions overall (Figs. 5b, 6b, 7b). It is likely these smaller events are related to the roiling of the lava lake. Assuming the monopole calculations serve as an adequate estimate, the number of explosions and total volume outflux per hour decreased rapidly between August 14–20, 2013 (Figs. 5b and 6b). Due to the numerous small amplitude events, this method suggests the eruption in February and August consisted of a mixture of small amplitude roiling of the lava lake and larger amplitude explosions from slug bursts.

The third method, HPSC, generally shows a smaller number of events occurred overall (Figs. 5c, 6c, and 7c). Results suggest a trend similar to that which is seen when implementing the BPSC method. This method also suggests the number of explosions and total volume outflux per hour decreased rapidly between August 14–20, 2013. However, the HPSC method finds fewer events with radii near zero (Fig. 7c). Therefore, the results from the HPSC method suggest the eruption was a mixture of roiling within the lava lake and larger slug burst explosions, but fewer events occurred overall.

As mentioned above, video observations show that roiling of the lava lake occurred in late August. We suggest this roiling can be modeled assuming a monopole source because it is essentially a combination of small bubble bursts. However, the nature of monopole source inversion suggests that it is likely that all methods underestimate the total volume of emissions. They do, however, provide a lower bound on the eruption emissions during mid February and mid to late August.

6.3. Implications for volume flux calculations

Infrasound-based inversions for volume flux using a monopole assumption have been commonly used, although a number of assumptions must typically be made. These include the assumption that the source radiates sound equally in all directions and that the sound travels as a plane-wave in a homogeneous half-space. The assumption that the sound radiates equally in all directions allows for the attenuation of acoustic amplitude as 1/r (where r is the distance from source to

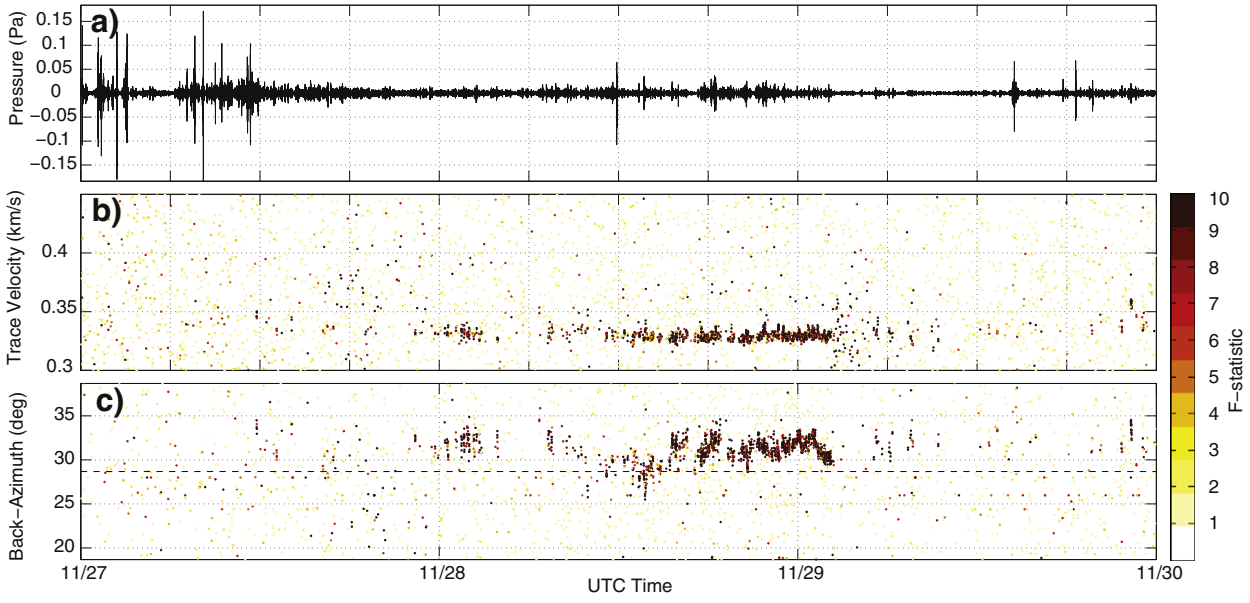

Fig. 8. Regional infrasound analysis for 27–30 November 2012. a) Infrasound data from IS44 filtered using a pure-state filter (Olson, 2004). b) trace velocity and c) back-azimuth for 20 s windows. Data segments are colored by the F-statistic, a measure of the SNR. Lava flows occurred from two centers and ash emissions were occurring at Tolbachik Volcano during this period (Gordeev et al., 2013a). The high SNR at this time along with the back-azimuths and trace velocities suggest that signals from Tolbachik Volcano were picked up at the IS44 array between November 28 00:00–early November 29. Late November 29–November 30 shows fewer events from Tolbachik Volcano. The lack of a signal at the eruption's onset (November 27 5:15 UTC) and after early November 29 suggests a smaller eruptive intensity during these times.

sensor). This is generally an adequate assumption when studying local infrasound unless significant topography is present (Fee and Matoza, 2013). This 1/r attenuation is in Eq. (1) as part of the spherical acoustic radiation pattern. Fig. 9a–c shows the WXC master waveforms and their corresponding mass and cumulative mass outfluxes from the February and August data. Since the sensor in February is located only ~100 m from the vent and the August sensors are located ~825–955 m from the vent, the amplitudes of events in August must be ~8.3–9.5 times smaller than those in February (i.e. their maximum amplitude must be less than 1.55–1.80 Pa) in order to obtain a similar cumulative mass outflux. While the master waveform from the data beginning August 14, 2013 fits the 1/r spreading rule, the master waveforms from the data beginning August 16 and August 19, 2013 are clearly greater than 1.80 Pa. Therefore, the calculations for the master waveforms from August 16 and 19 give greater values for total cumulative outflux. This phenomenon could explain why greater total volume outflux per hour (Fig. 6a) and larger average slug radii (Table 1) are seen in the August data when using the WXC method. However, we are confident that monopole source inversion is an adequate method to provide lower bounds on estimates of volume outfluxes for our data Therefore, we postulate that these larger amplitudes are due to local propagation effects, to the contribution of a non-monopole component during this period, or to a deviation from spherically symmetric radiation. However, understanding the local propagation effects, the contribution of a non-monopole component, and/or the radiation pattern requires a more robust infrasound sensor configuration.

Similar studies have been done at other volcanoes, including Mt. Erebus, Antarctica (Firstov and Kravchenko, 1996; Johnson et al., 2004; Johnson et al., 2008), Pacaya Volcano, Guatemala (Dalton et al., 2010), and Mt. St. Helens, USA (Moran et al., 2008). Data collected at Mt. Erebus, Antarctica by Johnson et al. (2008) displays slug burst signals with slight variations from the typical signal. This variation is likely due to some horizontal directional component of the source mechanism. Even so, explosions at Mt. Erebus between January 6–April 13, 2006 were modeled using a monopole source model and show the cumulative outflux values from each explosion ranged from <1000 kg to ~20,000 kg, with a median value of 5000 kg (Johnson et al., 2008). Results from Pacaya Volcano in 2010 produced smaller slug bursts that gave cumulative flux values ranging from 12 kg to 962 kg. Moran et al. (2008) also used a monopole source inversion method, but on a rockfall instead of a volcanic eruption. Results from the rockfall show a cumulative outflux of 7.5×10^6 kg, far larger than values calculated from the volcanic eruptions. Ranges in cumulative outflux values for individual slug bursts from our data are listed in Table 3. For all datasets and methods the Tolbachik slug bursts show a per event cumulative outflux range greater than that calculated from measurements at Pacaya, less than those calculated from measurements at Mt. Erebus, and far less than those calculated from a rockfall at Mt. St. Helens. From this, we determine the slug bursts at Tolbachik volcano during February and August 2013 must have been larger on average than those at Pacaya Volcano in 2010, but smaller on average than those at Mt. Erebus in 2008.

Our emissions estimates show general agreement with those estimated from satellite observations. Telling et al. (2015) make use of satellite observations to predict mass of SO_2 emissions during peak eruption periods from the 2012–2013 Tolbachik eruption. The time periods we use to estimate cumulative mass outflux of emissions from slug burst events fall either near to or within the peak periods identified by Telling et al. (2015). SO_2 emissions for the peak eruptive period in early February 2013 are estimated to be 3–3.5 kt during a range of 1–2 days (Telling et al., 2015). We estimate cumulative mass of emissions during February 12–14, 2013 to be 38 kt (Table 2). If we assume that SO_2 accounts for ~2.3% of the total emissions (Zelenski et al., 2014) then we can directly calculate the mass of SO_2 from our emissions estimates. We therefore estimate the amount of SO_2 emitted from February 12–14, 2013 to be 0.87 kt. As mentioned, estimates from satellite measurements are for a peak eruptive period lasting 1–2 days at the beginning of February 2013. Because our estimates correspond to emissions during mid-February it is likely that total emissions decreased slightly after the peak period of eruption identified. Therefore, our estimates for mass of emissions agree reasonably well with those estimated from satellite observations. We also compare our estimates from late August with those from satellite observations collected during the same time. Telling et al. (2015) estimate that less than 1.7 kt of SO_2 were emitted during the final two weeks of the eruption (August 16–30, 2013). Our estimates, converted to kt SO_2 in the same manner as before, range from 0.51–0.74, 0.25–0.39, and 0.069–0.25 kt for August 14, August 16, and August 19, respectively. The range in values is a result of the three different explosion picking methods used on the August data sets (Table 2). Cumulatively these add up to give a range of 0.83–1.4 kt SO_2. Estimates from satellite observations during the last two weeks are likely smaller than actual values due to the low plume altitude (Telling et al., 2015). Because SO_2 emissions estimates from satellite observations are likely larger, we determine that they are in general agreement with our estimates. This agreement supports the monopole source inversion as a potential method for estimating mass of emissions from slug burst events.

7. Conclusions

Both regional and local infrasound data were analyzed to track and characterize the eruption dynamics of Tolbachik Volcano. Regional data focused on the eruption onset in late November 2012, while local data focused on eruptive activity in February and August 2013. Regional data gives insight into the intensity of the eruption from the presence or absence of the eruption signal. The eruption at Tolbachik Volcano was likely less energetic at the onset (November 27, 2012) and gained intensity at the time when it is first seen at the IS44 array (late November 28–early November 29). After early November 29 the disappearance of the signal in the regional infrasound suggests that the eruption became less energetic once again. Three methods were employed to pick slug burst events from four local infrasound data, one in February and three in August. Each individual slug burst event was assumed to result from an acoustic monopole, allowing us to calculate the volume outflux and slug radius per event, as well as cumulative mass and total volume outfluxes per hour for each dataset. Comparison of event picking methods shows that regardless of the method, real slug burst events were identified. Estimated emissions outfluxes and slug radii distributions from the three methods provide three possible eruption styles for the eruption dynamics of Tolbachik Volcano from mid-February to late-August: 1) the eruption stays consistent through time, 2) the eruption transitions from dominantly slug bursts in February to a mixture of roiling within the lava lake and slug bursting in August and 3) the eruption transitions from dominantly slug bursts in February to a mixture of roiling within the lava lake and slug bursting in August, but fewer explosions occurring overall. While emissions outfluxes from the WXC method likely underestimate the actual total emissions from Tolbachik Volcano during the study time periods, they do provide a lower bound. Cumulative outflux of emissions per event in both February and August range from <100 to ~3000 kg for all methods. These values are greater than emissions calculated at Pacaya Volcano, but less than those calculated from emissions at Mt. Erebus Volcano (Table 2). From this, it is determined that slug bursts at Tolbachik Volcano in February and August were larger on average than those at Pacaya Volcano in 2010, but smaller on average than those at Mt. Erebus in 2008. We also find our emissions estimates agree well with those estimated from satellite observations during periods in February and August. This supports the use of monopole source inversion for estimating outflux of emissions from slug burst events.

Although the infrasound data collected from Tolbachik were adequate for the methods used in this paper, it is not unusual to suggest future studies of this sort that employ the use of more infrasound

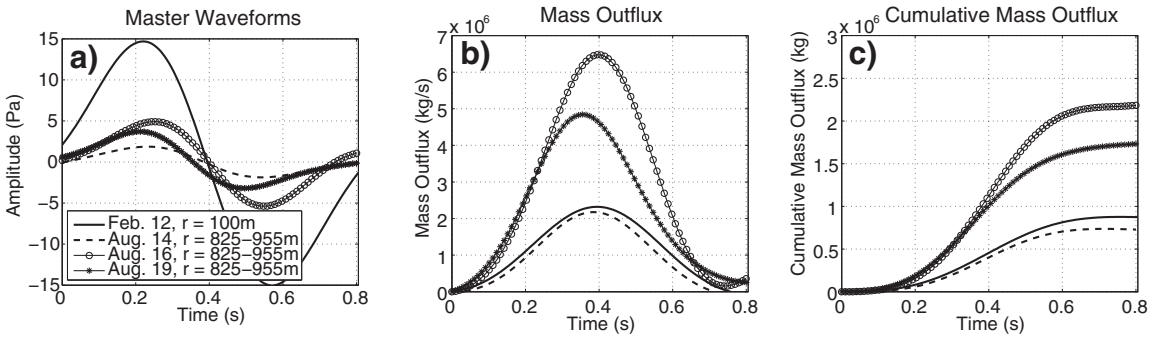

Fig. 9. Infrasound-derived mass outflux calculations for the selected master waveforms. Plots show a) pressure traces of master waveforms from each dataset (noted by its distance, *r*, from the vent), b) corresponding mass outflux calculations, and c) cumulative mass outflux calculations. To obey the 1/*r* spreading rule that describes the spherical acoustic radiation pattern based on distance from the source, the amplitudes of events in August must be ~8.3–9.5 times smaller than those in February (i.e. their maximum amplitude must be less than 1.55–1.8 Pa) in order to obtain a similar cumulative mass outflux. Only the dataset beginning August 14 has this relationship. This could explain why greater total volume outflux per hour and larger average slug radii are seen in the August data when using the WXC method. Larger amplitudes in the August data are possibly due to local propagation effects, the contribution of a non-monopole component, and/or a deviation from the assumed spherically symmetric acoustic radiation pattern.

sensors and attempt to place them in other configurations. Additional infrasound sensors, particularly in February, would have provided the ability to track changes from February to August solely using the BPSC and HPSC methods. In August the sensors were aligned towards the vent, which allowed for good temporal resolution. However, Johnson et al. (2008) and Kim et al. (2012) have shown that it is useful to place sensors around the vent in order to improve the spatial resolution and stability of the inversion. Using this configuration, one can investigate the possibility of a non-monopole component in the slug bursts. If such a component is found in the slug burst events, then a more complex source model would give more accurate source estimates.

Collecting gas measurements as a means to "calibrate" the monopole source inversion is also suggested. Dalton et al. (2010) show that making concurrent gas and acoustic measurements allows for a comparison between calculated and observed total emissions values. At Pacaya the results were promising, falling within an order of magnitude of one another. The results at Pacaya allow us to remain confident that our methods provide insight into the volume of emissions from slug burst events at Tolbachik Volcano during February and August 2013. However, obtaining a multiparameter dataset at Tolbachik Volcano would have allowed for emissions correlation, and would have likely supported the adequacy of the monopole source inversion method. Future work along these lines is suggested to validate infrasound-based emissions calculations.

Table 3
Comparison of cumulative outflux values from individual gas slug bursts at various volcanoes.

Volcano (and/or method)	Range of cumulative outflux values (kg)
Mt. Erebus 01/06/06–04/13/06	<1000–20,000
Pacaya	12–962
Mt. St. Helens Rockfall	7.5×10^6
Tolbachik Total (range of all data)	<100–3910
Tolbachik	<100–1539
02/12/13 05:53:32–02/14/13 23:26:08	
Tolbachik	
08/14/13 21:00:38–08/16/13 04:50:09	
WXC	<100–1805
BPSC	<100–1947
HPSC	<100–1802
Tolbachik	
08/16/13 21:29:09–08/17/13 21:29:09	
WXC	<100–1847
BPSC	<100–2352
HPSC	<100–2352
Tolbachik	
08/19/13 21:29:09–08/20/13 12:27:08	
WXC	<100–3048
BPSC	<100–3910
HPSC	<100–2072

Acknowledgments

Funding for this research was provided by the UAF Geophysical Institute and NSF EAR 1331084. Field work and assistance was provided by the Institute of Volcanology and Seismology (IVS) and the Kamchatka Branch Geophysical Surveys (KBGS). It is with sincerest thanks that we acknowledge our colleagues at the University of Alaska Fairbanks (UAF), KBGS and IVS. Their efforts were extremely helpful in data collection and interpretation.

References

Anstey, N.A., 1964. Correlation techniques — a review. Geophys. Prospect. 12 (4), 55–82.
Blandford, R.R., 1974. An automatic event detector at the Tonto Forest seismic observatory. Geophysics 39, 633–643.
Braitseva, O.A., Ponomareva, V.V., Sulerzhitsky, L.D., Melekestsev, I.V., Bailey, J., 1997. Holocene key-marker tephra layers in Kamchatka, Russia. Quat. Res. 47 (2), 125–139.
Brandeis, G.H., Ooi, W.L., Hossain, M., Morris, J.N., Lipsitz, L.A., 1994. A longitudinal-study of risk-factors associated with the formation of pressure ulcers in nursing-homes. J. Am. Geriatr. Soc. 42 (4), 388–393.
Buckingham, M.J., Garces, M.A., 1996. Canonical model of volcano acoustics. J. Geophys. Res. Solid Earth 101 (B4), 8129–8151.
Dalton, M.P., Waite, G.P., Watson, I.M., Nadeau, P.A., 2010. Multiparameter quantification of gas release during weak Strombolian eruptions at Pacaya Volcano Guatemala. Geophys. Res. Lett. 37.
Donn, W.L., Rind, D., 1972. Microbaroms and the temperature and wind of the upper atmosphere. J. Atmos. Sci. 29, 156–172.
Fedotov, S.A., Utkin, I.S., Utkina, L.I., 2011. The peripheral magma chamber of Ploskii Tolbachik, a Kamchatka basaltic volcano: activity, location and depth, dimensions, and their changes based on magma discharge observations. J. Volcanol. Seismol. 5 (6), 369–385.
Fee, D., Matoza, R.S., 2013. An overview of volcano infrasound: from Hawaiian to Plinian, local to global. J. Volcanol. Geotherm. Res. 249, 123–139.
Firstov, P.P., 1996. Wave disturbances in the atmosphere as a source of information on the dynamics of volcanic eruptions. Eos 318 (3), 813.
Firstov, P.P., Kravchenko, N.M., 1996. Estimation of the amount of explosive gas released in volcanic eruptions using air waves. Volcanol. Seismol. 17, 547–560.
Garces, M., Iguchi, M., Ishihara, K., Morrissey, M., Sudo, Y., Tsutsui, T., 1999. Infrasonic precursors to a Vulcanian eruption at Sakurajima Volcano, Japan. Geophys. Res. Lett. 26 (16), 2537–2540.
Gordeev, E.I., Murav'ev, Y.D., Samoilenko, S.B., Volynets, A.O., Mel'nikov, D.V., Dvigalo, V.N., 2013a. The Tolbachik Fissure Eruption of 2012–2013: preliminary Results. Dokl. Earth Sci. 452 (2), 1046–1050.
Gordeev, E.I., Muravyov, Y.D., Samoylenko, S.B., Volynets, A.O., Melnikov, D.V., Dvigalo, V.N., Melekestsev, I.V., 2013b. First results from the 2012–2013 Tolbachik fissure eruption. Bull. Volcano. Soc. Japan 58 (2), 1–8.
Green, D.N., Neuberg, J., 2005. Seismic and infrasonic signals associated with an unusual collapse event at the Soufriere Hills volcano, Montserrat. Geophys. Res. Lett. 32 (7).
Gresta, S., Ripepe, M., Marchetti, E., D'Amico, S., Coltelli, M., Harris, A.L.J., Privitera, E., 2004. Seismoacoustic measurements during the July–August 2001 eruption of Mt. Etna volcano, Italy. J. Volcanol. Geotherm. Res. 137 (1–3), 219–230.
Hagerty, M.T., Protti, M., Schwartz, S.Y., Garces, M.A., 2000. Analysis of seismic and acoustic observations at Arsenal Volcano, Costa Rica. J. Volcanol. Geotherm. Res. 121 (1–2), 15–63.

Inbar, M., Gilichinsky, M., Melekestsev, I., Melnikov, D., Zaretskaya, N., 2011. Morphometric and morphological development of Holocene cinder cones: a field and remote sensing study in the Tolbachik volcanic field, Kamchatka. J. Volcanol. Geoth. Res. 201 (1–4), 301–311.
Johnson, J.B., Ripepe, M., 2011. Volcano infrasound: a review. J. Volcanol. Geotherm. Res. 206 (3–4), 61–69.
Johnson, J.B., Aster, R.C., Ruiz, M.C., Malone, S.D., McChesney, P.J., Lees, J.M., Kyle, P.R., 2003. Interpretation and utility of infrasonic records from erupting volcanoes. J. Volcanol. Geotherm. Res. 121 (1–2), 15–63.
Johnson, J.B., Aster, R.C., Kyle, P.R., 2004. Volcanic eruptions observed with infrasound. Geophys. Res. Lett. 31 (14).
Johnson, J., Aster, R., Jones, K.R., Kyle, P., McIntosh, B., 2008. Acoustic source characterization of impulsive Strombolian eruptions from the Mount Erebus lava lake. J. Volcanol. Geotherm. Res. 177, 673–686.
Kim, K., Lees, J.M., Ruiz, M., 2012. Acoustic multipole source model for volcanic explosions and inversion for source parameters. Geophys. J. Int. 191 (3), 1192–1204.
Lighthill, J., 1978. Waves in Fluids. Cambridge University Press, New York.
Moran, S.C., Matoza, R.S., Garces, M.A., Hedlin, M.A.H., Bowers, D., Scott, W.E., Sherrod, D.R., Vallance, J.W., 2008. Seismic and acoustic recordings of an unusually large rockfall at Mount St. Helens, Washington. Geophys. Res. Lett. 35 (19).
Olson, J.V., 2004. The application of the Pure-State Filter to infrasound array data. Inframatics Newsl. 7, 15–21.
Petersen, T., 2007. Swarms of repeating long-period earthquakes at Shishaldin Volcano, Alaska, 2001–2004. J. Volcanol. Geotherm. Res. 166 (3–4), 177–192.
Petersen, T., McNutt, S.R., 2007a. Seismo-acoustic signals associated with degassing explosions recorded at Shishaldin Volcano, Alaska, 2003–2004. Bull. Volcanol. 69 (5), 527–536.
Petersen, T., McNutt, S.R., 2007b. Seismo-acoustic signals associated with degassing explosions recorded at Shishaldin Volcano, Alaska, 2003–2004. B. Volcanol. 69 (5), 527–536.
Ruiz, M., Lees, J.M., Johnson, J.B., 2006. Source constraints of Tungurahua volcano explosion events. Bull. Volcanol. 68 (5), 480–490.
Szuberla, C.A.L., Olson, J.V., 2004. Uncertainties associated with parameter estimation in atmospheric infrasound arrays. J. Acoust. Soc. Am. 115 (1), 253–258.
Telling, J., Flower, V.J.B., Carn, S.A., 2015. A multi-sensor satellite assessment of SO_2 emissions from the 2012–13 eruption of Plosky Tolbachik volcano, Kamchatka. J. Volcanol. Geotherm. Res. 307, 98–106.
Ulivieri, G., Ripepe, M., Marchetti, E., 2013. Infrasound reveals transition to oscillatory discharge regime during lava fountaining: implication for early warning. Geophys. Res. Lett. 40 (12), 3008–3013.
Vergniolle, S., Boichu, M., Caplan-Auerbach, J., 2004. Acoustic measurements of the 1999 basaltic eruption of Shishaldin volcano, Alaska — 1. Origin of Strombolian activity. J. Volcanol. Geotherm. Res. 137 (1–3), 109–134.
Yamasato, H., 1998. Nature of infrasonic pulse accompanying low frequency earthquake at Unzen Volcano, Japan. Bull. Volcanol. Soc. Japan 43, 1–13.
Zelenski, M., Malik, N., Taran, Y., 2014. Emissions of trace elements during the 2012–2013 effusive eruption of Tolbachik volcano, Kamchatka: enrichment factors, partition coefficients and aerosol contribution. J. Volcanol. Geotherm. Res. 285, 136–149.